Theoretical and Applied Climatology (2020) 141:229–246
https://doi.org/10.1007/s00704-020-03181-9

ORIGINAL PAPER

Industrial heat island: a case study of Angul-Talcher region in India

Manju Mohan[1] · Vivek Kumar Singh[1] · Shweta Bhati[1] · Neelesh Lodhi[2] · Ankur Prabhat Sati[1] · Nihar Ranjan Sahoo[3] · Simanchala Dash[3] · P. C. Mishra[4] · Sagnik Dey[1]

Received: 22 May 2019 / Accepted: 5 March 2020 / Published online: 16 April 2020

Abstract

Most of the urban heat island (UHI) studies are carried out in densely populated cities but core industrial areas are also potential sites of heat island effect despite having a comparatively lower population. In the present study, heat island assessment has been carried out for Angul-Talcher industrial area (ATIA) which is one of the oldest industrial areas of India and is still undergoing a transformation to accommodate more industries and mining operations. As the major contributors towards influencing local meteorology were expected to be industrial (and mining) activities, the heat island was studied as "industrial heat island" (IHI) rather than urban heat island. Industrial and mining sites were the most frequent nighttime canopy-layer heat island intensity (HIN) hotspots due to anthropogenic heat of associated industrial processes as well as built structures. During the daytime, croplands experienced the most frequent canopy-layer HIN hotspots which could be attributed to low moisture of the soils during the non-farming period of the field campaign. Hourly maximum atmospheric heat island intensities were observed in the range of 7–9 °C. Monthly maximum HINs ranged from 2.97 to 4.04 °C while 3-month mean HINs varied from 1.45 to 2.74 °C. Amongst different land use/land cover classes, the highest mean canopy-layer heat island intensity for the entire 3-month-long duration of field campaign during nighttime was assessed at the mining sites (3-month mean 2.74 °C) followed in decreasing order by the industrial sites (2.52 °C), rural and urban settlements (2.13 °C), and croplands (2.06 °C). Corresponding daytime canopy-layer heat island intensity was highest for the croplands (2.07 °C) followed in decreasing order by the mining sites (1.70 °C), rural and urban settlements (1.68 °C), and industry (1.45 °C).

1 Introduction

The weather pattern of most of the major cities around the world is changing gradually. A major cause of changing the weather is a change in urban land use patterns (Zhou and Chen 2018). Urban heat island (UHI) is a serious environmental issue caused by urbanization and human activities and might result in a change in the weather patterns. UHI phenomenon is observed in terms of temperature difference of air or land surface of an urban area with the rural or lesser developed area (Oke 1973; Montavez et al. 2000; Peron et al. 2015; Mohan et al. 2013). This temperature difference, known as urban heat island intensity, is generated due to certain features specific to urban areas such as low evaporation, growing anthropogenic heat, lower air circulation, pollution, city size, impervious surface, construction materials, and human activities (Morini et al. 2017). UHIs are observed based on the observation collected using in situ (stationary field survey, mobile survey, and weather monitoring stations) and satellite data (MODIS/Landsat data product) (Sahu et al. 2014). UHI can be classified based on the type of observation used to measure UHI. In situ observations are measured in the air as well as on surface while satellite-based data products commonly are used to derive land surface temperatures. UHI can be categorically divided into three types: canopy-layer UHI, boundary layer UHI, and surface layer UHI. Canopy-layer UHI is measured up to the height of the building whereas boundary layer UHI is measured above the height of the building. Surface layer UHI is measured on the surface and surface temperature is hotter

✉ Manju Mohan
mmohan66@gmail.com; mmanju@cas.iitd.ac.in

[1] Centre for Atmospheric Sciences, Indian Institute of Technology Delhi, Hauz Khas, New Delhi 110016, India

[2] Environmental Sciences and Biomedical Metrology Division, CSIR-National Physical Laboratory, Dr. K. S. Krishnan Marg, New Delhi 110012, India

[3] Odisha State Pollution Control Board, Nilakantha Nagar, Bhubaneswar, Odisha 751012, India

[4] Visiontek Consultancy Services Pvt Ltd., Chandaka Industrial Estate, Bhubaneswar, Odisha 751024, India

than air temperature (Mallick et al. 2013; Joshi et al. 2015). Table 1 lists canopy UHI observed in major cities of the world with its population (Mohan et al. 2013).

Santamouris (2015) reported data of UHI and characteristics for 101 Asian and Australian cities and regions. The magnitudes of the average annual, average maximum, and absolute maximum intensities were 1.0 °C, 3.1 °C, and 6.2 °C. About 58% of the studies reported an average annual UHI intensity lower than 1 °C, while 55% of the articles presented an average maximum UHI intensity lower than 5 °C. Thirty percent of the studies presented an absolute maximum UHI intensity below 5 °C, while for 20% of the studies, the maximum UHI magnitude exceeded 8 °C.

In India, UHI studies have been conducted mainly in the past two decades. These studies are usually focused on metropolitan cities as shown in Table 2.

UHI studies have mostly focused on highly populated cities having urban infrastructures such as housing, offices, and commercial complexes. However, core industrial zones can also be equally impacted and are vulnerable to the UHI effect owing to the high anthropogenic emissions from various industries. These industrial zones are the center of economic growth, but they are not densely built-up like developed cities and in India are usually away from dense population centers. However, industrial processes, as well as building infrastructure in industrial regions, have the potential to influence the local microclimate. Some factors that could contribute towards alteration in local microclimate include high industrial emission from different large- and small-scale industries, vehicular movement within and outside industrial premises, and fuel and electricity consumption for residential and industrial purposes.

With this background, the prime objective of the present work is to study heat island effect in an industrial region of India, namely Angul-Talcher industrial zone in the state of Odisha. The heat island effect has been studied as an industrial heat island (IHI). Angul-Talcher region constitutes some of the oldest industrial setups and is an economic growth center for Odisha state as the region has a huge deposit of coal as a mineral. Industrialization and mining activities have been known to be one of the major causes of pollution in this region because of opencast mines, aluminum smelting, thermal power generation, steel plants, and many more. The analysis in this study is based on observations of a field campaign conducted during April–July 2016, details of which are presented in Section 2. This is the first elaborate and extensive field campaign in India and amongst few in the world to examine heat island effect in a core industrial area.

2 Study area and field campaign

2.1 Study area

Angul-Talcher region is one of the oldest industrial zones of the country. It is centrally located and 120 km away from Bhubaneswar, the capital city of Odisha. Geographically, the study area is located between latitudes 20° 41′ 10″ N and 21° 08′ 37″ N and longitudes 84° 55′ 00″ E to 85° 30′ 00″ E. Brahmani River divides the region into 2 halves from north to west and drains directly into the sea of Bay of Bengal. As mentioned earlier, Angul-Talcher region is one of the earliest industrialized regions of India. Setting up of heavy industry started in Angul-Talcher in the early nineteenth century with

Table 1 UHI studies around the major cities of the world with observed UHI intensity

Cities	Population ($\times 10^6$)	Country	UHI intensity observed	Source
New York	19.86	USA	Maximum of 10 °C during nighttime	Ramamurthy et al. (2017)
Paris	2.2	France	Maximum of 6 °C	Sarkar and De Ridder (2011)
Toronto	2.8	Canada	Maximum of 9 °C	Wang et al. (2016); Wang et al. (2015)
Rotterdam	6.24	Netherlands	Maximum of 4.3 to 8 K	van Hove et al. (2015)
Cologne	1	Germany	Maximum of 5 K	Zhu et al. (2015)
Beersheba	0.2	Israel	Varying from 0.8 to 3.1 °C	Saaroni and Ziv (2010)
Kraków	0.7	Poland	Varying from 1.6 to 6.6 K (across the city)	Bokwa et al. (2015)
California	39.5	USA	Maximum of 5 °C	Taha (2017)
Wuhan	10.6	China	Maximum of 3 °C	Li et al. (2012)
Adelaide	1.2	Australia	Maximum of 6 °C	Soltani and Sharifi (2017)
Birmingham	1.06	England	Varying from 1.7 to 3.2 °C	Azevedo et al. (2016)
Cologne	1.05	Germany	Maximum of 5 °C	Zhu et al. (2015)
London	8.7	England	Maximum of 1.5 °C	Barlow et al. (2015)
Enugu	0.72	Nigeria	Maximum of 6 °C	Christian (2013)

Table 2 UHI studies around the major cities of India with observed UHI intensity

Cities	Indian state	UHI intensity observed	Source
Delhi	Delhi	Varying between 4 and 7 °C	Mohan et al. (2009), Mohan et al. (2012), Pandey et al. (2012), Mallick et al. (2013), Mohan et al. (2013), Grover and Singh (2015), Babazadeh and Kumar (2015), Yadav et al. (2017)
Mumbai	Maharashtra	Maximum of 3 °C	Srivastava et al. (2016), Maral and Mukhopadhyay (2015)
Ahmedabad	Gujarat	Varying between 1.5 and 2 °C	Joshi et al. (2015), Mathew et al. (2015)
Bangalore	Karnataka	Maximum of 2.5 °C	Sastry et al. (2017)
Chennai	Tamil Nadu	Maximum of 2.5 °C in summer and 3.35 °C in winter	Amirtham (2016)
Pune	Maharashtra	Above 2 °C	Parishwad and Shinkar (2017)
Bhubaneswar	Odisha	Above 1.7 °C	Swain et al. (2017)
Kolkata	West Bengal	Above 2 °C	Khan and Chatterjee (2016)

the discovery of coalfields in 1837. The region has 4106 industries ranging from small to large scale and is listed amongst the 43 most polluted industrial clusters in India. Further, it is ranked 7th amongst the critically polluted zones evaluated by the Central Pollution Control Board (CPCB), [CPCB, 2010]. Presently, there are several thermal power plants, steel and aluminum plants, and mining industries in the area like Talcher Thermal Power Station (NTPC), NTPC Kaniha, Jindal Steel and Power Ltd. (JSPL), Jindal India Thermal Power Ltd. (JITPL), Mahanadi Coal Field Ltd., and Lingaraj coal mines.

2.2 Field campaign

An area of 3000 km^2 was considered for the present study. The area was chosen so as to include all core industrial and mining spots, as well as major land use/land cover (LULC) features within Angul-Talcher region. The topography of Angul-Talcher region has hills in the north and industrial setup along with tributaries of Brahmani River in the south. Opencast mining is carried out in the central part of the region and the rest of the region is plain and usually covered with forests and agriculture fields. The field campaign was carried out for 3 months starting from April 15, 2016, to July 14, 2016. Thus, the observation period covered days for both summer and monsoon season. In situ observations were collected during the field campaign for near-surface temperature (Ta), relative humidity, and land surface temperature (Ts).

2.3 Instrument details

Fifty micrometeorological stations were set up throughout the study area. Sensors for air temperature and relative humidity were kept inside a shield mounted on an iron rod at about 2 m height while a land surface temperature (LST) sensor was secured on the ground surface. All three sensors were connected to a data logger (Watchdog Model 1400) and also fixed on the pole, which stored data averaged on an hourly basis for analysis. The instruments were installed such that the immediate surroundings at least up to 10 m or more from the instrument were open and not obstructed by any tree or building.

The list of parameters and details of the sensors are as follows:

(I) Air temperature (AT) sensor (with radiation shield)

Range − 40 to + 85 °C
Accuracy ± 0.5 °C within the range − 20 to 50 °C; ± 0.25 to 0.4 °C within active plant growth temperature range of 5 to 40 °C and ± 0.5 °C beyond this range
Resolution 0.1 °C

(II) Relative humidity (RH) sensor

Range 0 to 100%
Accuracy ± 3% at 25 °C within the range − 20 to 50 °C
Resolution ± 0.1%

(III) Skin temperature at the surface (SST) sensor

Range − 20 to 70 °C
Accuracy ± 0.5 °C within the range − 20 to 50 °C; ± 0.25 to 0.4 °C within active plant growth temperature range of 5 to 40 °C and ± 0.5 °C beyond this range
Resolution 0.1 °C

In addition, fixed tower weather stations were installed at select locations at a height of 10–15 m to give information about various other meteorological parameters such as wind speed and direction, dry bulb temperature, atmospheric pressure, and solar radiation. Data of five weather stations (WS)

already operating in various industries in the study area, namely, at NALCO captive power plant, NTPC Kaniha, NTPC Talcher, and two stations at Bhushan Steel Plant were also utilized for the study. In addition to these existing weather stations, two more weather stations were set up at rural sites (Baghamunda and Saradhapur). Further, specific weather events such as rainfall, dust storms, and thunderstorms were also recorded during the sampling period.

2.4 Station selection and classification

Stations for observations were selected with the consideration that all different types of land use/land cover (LULC) pattern within the study area is included. Landsat 8 data product of 22 March 2016 was used for the preparation of the LULC classification map of Angul-Talcher region. Major LULC classes within the study area are forests, industry, cropland, mining, barren, urban and rural settlements, and water bodies as shown in Fig. 1. Table 3 lists different types of LULC classes, the number of stations in each LULC, and the name of each station.

2.5 Weather conditions during the field campaign

The climate of Angul-Talcher region is generally dry and semi-arid but changes during monsoon season where there is high precipitation. Hot summer months prevail from March to June where maximum temperatures are close to 48–50 °C. Conditions during summer in mining areas are worse because of mine fire which is used as a technique for opencast mining (Jha 2015) which contributes further in the extreme weather (Mishra and Das 2017). The temperature in winter months (December–January) drops to 5 °C whereas in monsoon season (June to September), the temperature is varying from 30 to 40 °C.

The duration of the field campaign spanned over summer and early monsoon in the study area. Rainfall events started with the second half of the month of June. Rain events occurred almost 5 days a week during the month of July. Consequently, temperatures decreased successively every month. Table 4 shows the range of air and surface temperatures for every week of the field campaign.

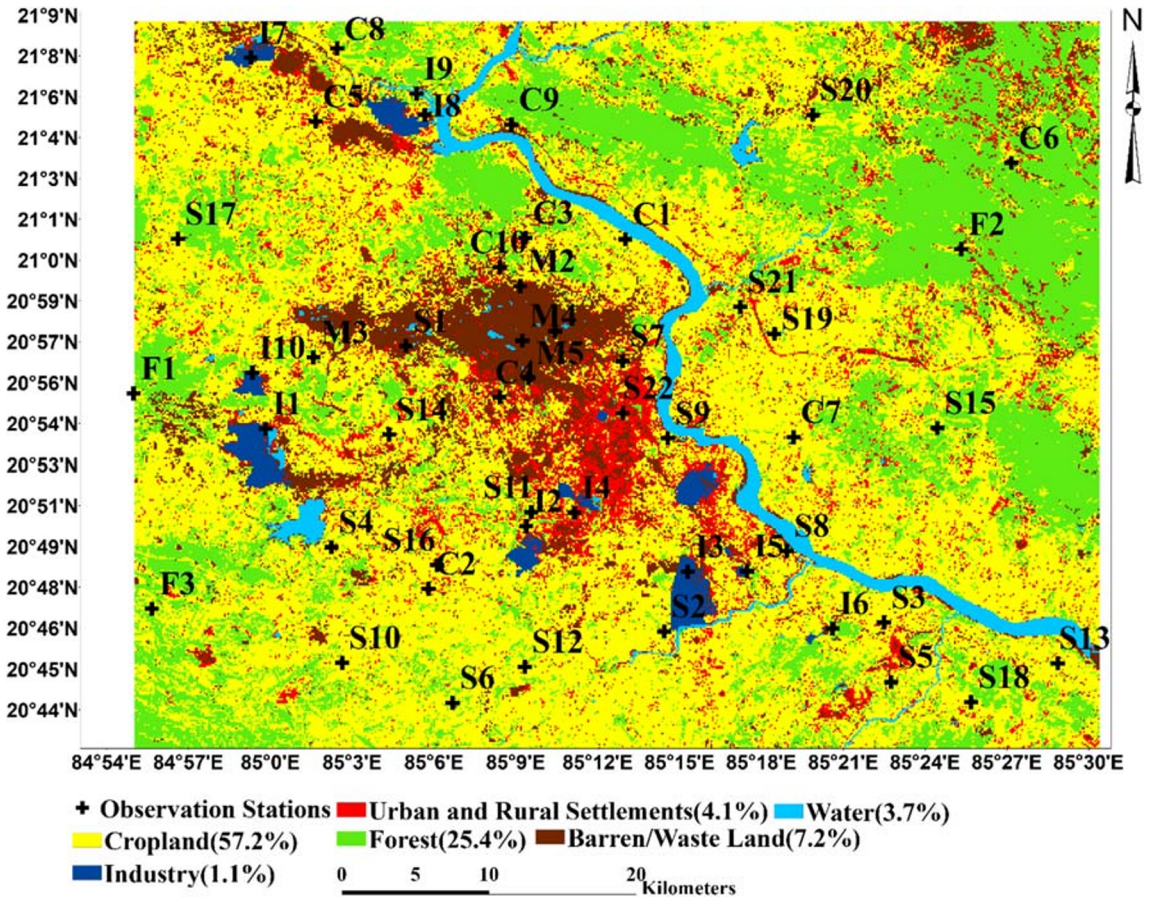

Fig. 1 Study area of Angul-Talcher along with distribution of monitoring stations [I industry, M mining, S rural and urban settlements, C croplands, F forests]

Table 3 Observation stations of the field campaign

S. no.	LULC	Area covered (%)	Total number of stations	Station name	Station number
1	Forest	25.4	3	TangiriSahi	F1
				Baghamunda	F2
				Saradhapur	F3
2	Industry	1.1	10	JSPL	I1
				Nalco Smelter	I2
				Bhushan	I3
				Nalco Captive Power Plant	I4
				Naba Bharat Venture	I5
				MGM Steel Power Plant	I6
				Jindal Thermal JITPL	I7
				NTPC Kaniha Himgiri	I8
				NTPC Kaniha EDC	I9
				Monnet Power Company Limited	I10
3	Cropland	57.2	10	Sirigida	C1
				Naugaon	C2
				Godibandha	C3
				Gobara	C4
				Kansamunda	C5
				Patharagarh	C6
				Kataraparha	C7
				Jharaberini	C8
				Dangaraberha	C9
				Ranganatia	C10
4	Mining	1.2	5	Lingaraj	M1
				Bharatpur North	M2
				Hingula	M3
				Bhubaneswari Coal Mining Ltd	M4
				South Balanda	M5
5	Urban-rural settlement	4.1	22	Balrampur	S1
				Purunakot	S2
				Dhaulpur	S3
				Rantalei	S4
				HandiPhuta	S5
				Bashala	S6
				BaghuaBol	S7
				Kharhagaprasad	S8
				Dasanali	S9
				Lacchabandha	S10
				Nalco Guest House	S11
				Phulaparha	S12
				GailoBelaparha	S13
				Kuio Jamunali	S14
				Kendutola	S15
				Angul-Khaleri	S16
				Kosala CMPDI Camp	S17
				Bahandei	S18
				Singarha	S19
				Chandapur	S20
				Rangathali	S21
				NTPC-TTPS Guest House	S22
6	Barren/wasteland	7.2	---	---	---
	Total	100	50		

3 Methodology

Twenty-two urban and rural settlements stations, ten industry stations and five mining stations in the Angul-Talcher region were used to study atmospheric and surface IHIs as mentioned in Table 3 and shown in Fig. 1. Percentage cover of the impervious surface and vegetation around the station was calculated using LULC derived from Landsat data product of 30-m resolution (Li et al. 2015; Song et al. 2016; Zhang and Weng 2016). Built-up regions in this study are categorized as Industry and urban and rural settlements which are explained as follows:

a. Industrial stations

Industries are made of metal, steel, and concrete construction material. These areas have no or few trees and plants in

Table 4 Maximum and minimum temperatures during field campaign

Week	Period (year 2016)	Air temperature (°C)		Surface temperature (°C)	
		Maximum	Minimum	Maximum	Minimum
1	15 Apr to 21 Apr	47.5	23.9	65.0	25.1
2	22 Apr to 28 Apr	48.1	24.8	64.9	25.0
3	29 Apr to 05 May	47.3	23.5	64.8	24.8
4	06 May to 12 May	46.1	23.4	64.7	24.8
5	13 May to 19 May	44.5	23.3	64.6	24.8
6	20 May to 26 May	44.4	23.3	61.5	24.7
7	27 May to 02 Jun	43.7	22.9	61.4	24.5
8	03 Jun to 09 Jun	43.5	22.8	61.1	24.4
9	10 Jun to 16 Jun	42.9	22.8	60.2	24.3
10	17 Jun to 23 Jun	40.3	22.8	57.8	24.3
11	24 Jun to 30 Jun	40.0	22.6	55.9	24.1
12	01 Jul to 07 Jul	37.5	22.5	46.7	24.0
13	08 Jul to 14 Jul	34.3	22.4	43.0	23.8

and around the industry. It consists of high- and mid-rise buildings like towers and stacks. The percentage of impervious surface in the industrial stations varies from 70 to 90% and vegetation cover by 20 to 40%.

b. Urban and rural settlements

Residential (urban and rural) area is categorized into urban and rural settlements where urban areas are areas with open mid-rise buildings with an abundance of low and scattered trees. Impervious surface range varies from 50 to 70% whereas vegetation cover by 30 to 50%. Rural settlement areas are areas with 40 to 50% impervious surface and 55 to 70% vegetation.

Other LULCs in which stations are located are mining, cropland, and forest areas. These land cover types have few or no buildings in and around stations. In forests, more than 90% of the area is covered by low- and high-rise trees with no anthropogenic heat. Mining stations are bare soil or sands with few or no trees. Mining stations generate substantial anthropogenic heat because of the mining operations. A large area of the Angul-Talcher region is under croplands which is used for agricultural activities and cultivating trees and plants. It has more than 90% of vegetation cover during crop seasons (July–February) and the land remains dry during the rest of the months (March–June) with little natural and cultivated vegetation.

Urban heat island is defined as the temperature difference between an urban area and a nonurban area. An urban area is described as an area that is characterized by built-up structures and human activity which are absent or minimal in nonurban areas and could usually be forests or croplands.

Likewise, in the present study, industrial heat island is estimated as

$$\mathrm{IHI} = T_{\mathrm{site}} - T_{\mathrm{forest}}$$

Heat island intensity (HIN) has been estimated with reference to forests. According to Wang et al. (2017), for considering forest as a reference station, the percentage cover of trees and plants should be more than 90%, no impervious surface in and around the station and away from all industry, urban and rural settlement, and mining. These conditions were satisfied by three forest stations in the study area. These three forest stations (F1, F2, and F3 as mentioned in Table 3) were in three different directions in Angul-Talcher region as shown in Fig. 1. Forest stations were relatively amongst the least temperature stations usually. Thus, the average temperature of all three stations is considered representative of a typical "forest" station as reference for estimating the IHI magnitude over the study region. The period of the study is divided into 3 months (a) April 15–May 14, 2016, as summer month; (b) May 15–June 14, 2016, as late summer to early monsoon month; and (c) June 15–July 14, 2016, as monsoon season.

Satellite-derived land surface temperature is widely used for estimation of UHI since the late 1970s and particularly for studying daytime and nighttime variation of land surface temperature (Wang et al. 2017). In many studies, MODIS Terra and Aqua satellite data product of 1-km resolution are used for estimation of UHI (Weber et al. 2015; Hu and Brunsell 2015; Sismanidis et al. 2015; Kikon et al. 2016; Bokaie et al. 2016; Tran et al. 2006; Toparlar et al. 2015; Wang and Akbari 2015; Tomlinson et al. 2012; Zhibin et al. 2015; Xie and Zhou 2015). Many UHI studies also evaluate the role of NDVI (Normalized Difference Vegetation Index), solar radiation, evapotranspiration, and many more using MODIS satellite data product (Leconte et al. 2015; Tan et al. 2015; Kaplan et al. 2018; Van Nguyen et al. 2015; Gallo 2002; Weber et al. 2015). In this study, in situ LST-based HINs have been compared with MODIS 8-day derived LST-based surface HINs.

4 Results and discussion

4.1 Atmospheric IHIs

Figure 2 displays box plots of heat island intensities for different LULCs for 3 months of field campaign during nighttime hours (2200–0300 h local time). The box represents the interquartile range; that is, the first quartile to the third quartile and the line within the box denotes the median. Ends of the line going through the box indicate minimum and maximum. The dots inside the box represent the mean value.

It can be seen that mining stations showed the highest mean HINs during nighttime followed by industrial stations for the entire duration of observations. Settlements and croplands have lower HINs. Individually, the mining station of Lingraj (M1) observed the highest hourly nighttime HIN with the maximum value being 7.6 °C. Other stations with higher HINs were industrial stations of JSPL (I1; 7.5 °C), Bhushan Steel (I3; 6.5 °C), and Nava Bharat (I5; 6.1 °C).

While the minimum and maximum values exhibit varying behavior amongst different LULCs, it should be noted that quartiles of both industries and mining stations are always higher than settlements or croplands. This indicates that not just average values but even the frequency of higher HINs is higher in industries and mining stations. Further, we can see that HINs are highest in the first month and continuously decrease until the third month with the emergence of monsoons.

The behavior of these LULC changes during daytime as depicted in Fig. 3. On average, croplands exhibit higher HINs in comparison with industrial and mining sites. Maximum hourly HINs for individual stations are observed at croplands such as Jharaberini (C8; 10.6 °C), Kataraparha (C7; 9.8 °C), and Kansamunda (C5; 9.2 °C) and settlements of Chandapur (S20; 10.2 °C), Gailo Belaparha (S13; 10.1 °C), and Dhaulpur (S3; 9.7 °C). Overall HINs have decreased from the first month to the third month.

Figure 4 displays a diurnal profile of heat island intensity of four LULCs averaged over the period of the first month. It can be seen that croplands start experiencing higher temperatures (and hence higher HIN) before other LULCs from 0700 h while industrial and mining stations are still experiencing cooling at this hour. Daytime comparatively has higher HIN over croplands while during nighttime, comparatively higher HIN is observed over mining and followed by the industrial sites. The field observations were carried out during non-active farming time due to which soils in croplands were dry thereby having high soil heat flux. Further, lower thermal admittance of rural lands, presence of moisture in industrial/built-up areas, and differential heating of rural and urban boundary layer leads to higher temperatures and substantial heat island intensities in rural areas as discussed further in Section 4.2. One more notable feature is the similarity between the profile of croplands and settlements. Largely, this is because settlements in Angul-Talcher are predominantly rural (which has less built structures than large cities) and are either surrounded by or close to the croplands.

The spatial variation of heat island intensities for the first month of the field campaign has been shown in Fig. 5. There is a prominent hotspot formed by industrial stations of JITPL (I7) and NTPC Kaniha (I9). There is also a hot zone centered at the mining region of Lingaraj mines (M1), Bhubhaneswari Mines (M4), and South Balanda mines (M5). The other prominent hotspot is around the industrial site of Bhushan (I3). As shown earlier, croplands experience higher HINs during daytime which can be seen in the spatial variation also. It can be seen from the figure that there is a prominent hot zone spread around Sirigida (C1), Godibanda (C3), Dangarbera (C9), and Chandapur (S20). Hotspots are also observed around settlements such as Dhaulpur (S3) and Phulapara (S12).

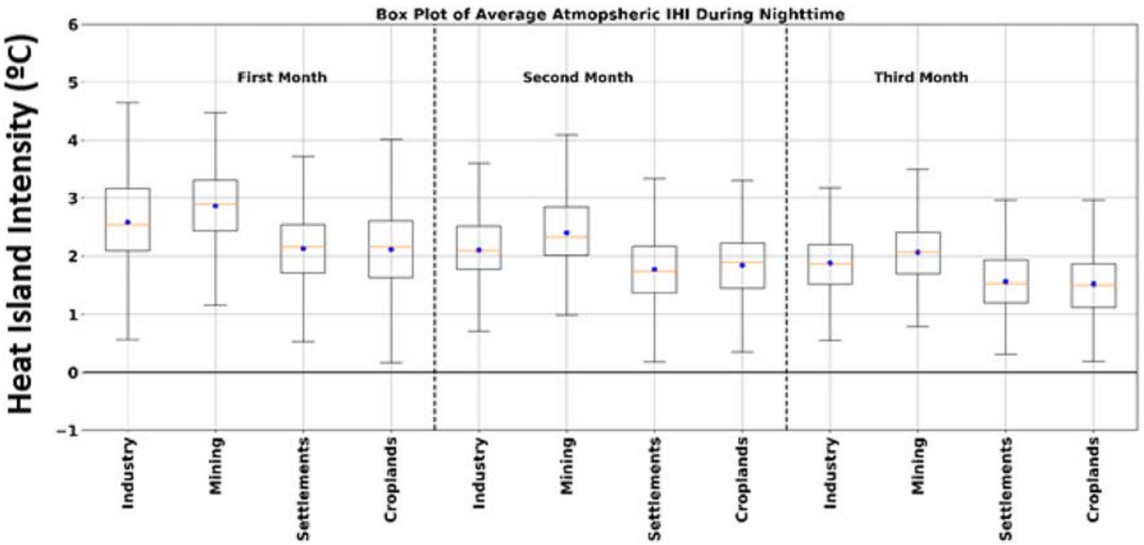

Fig. 2 Box plot of in situ industrial atmospheric heat island intensity over Angul-Talcher region during nighttime for different LULCs [first month: 15 April–14 May 2016, second month: 15 May–14 June 2016, third month: 15 June–14 July 2016]

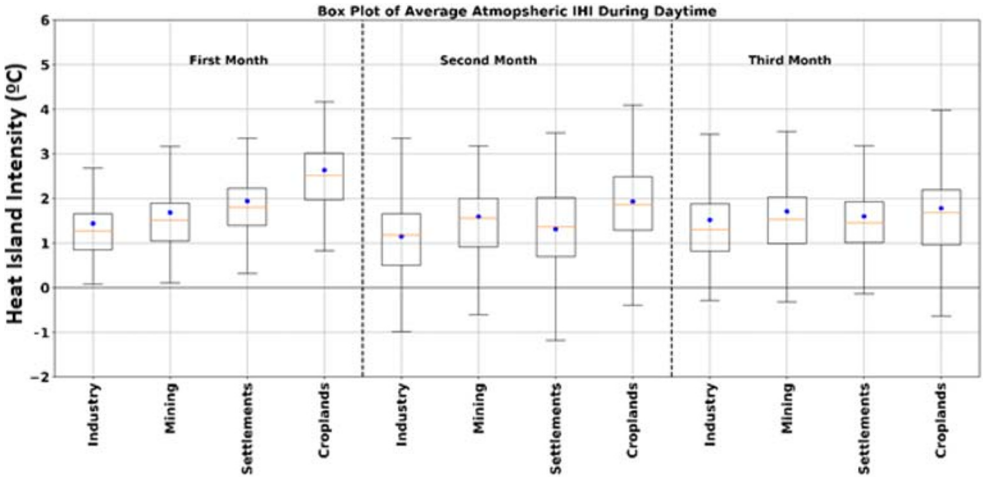

Fig. 3 Box plot of in situ industrial atmospheric heat island intensity over Angul-Talcher region during daytime for different LULCs [first month: 15 April–14 May 2016, second month: 15 May–14 June 2016, third month: 15 June–14 Jul 2016]

4.2 Major factors attributing to higher HINs over different LULCs during day/night

The heat balance equation at surface is:

$$Q^* + \mathrm{QH} + \mathrm{QE} + \mathrm{QS} + \mathrm{QA} + \mathrm{QP} = 0 \ \left(\mathrm{W\ m^{-2}}\right)$$

Q^*: the net radiation (sum of all short and long wave radiation fluxes)
QH: the sensible heat flux density (temperature)
QE: the latent heat flux density (evapotranspiration)
QS: the storage heat flux density/ground heat flux density
QA: the anthropogenic heat flux density
QP: the photosynthetic heat flux density (usually negligible)

Parlow et al. (1996) measured fluxes at different sites in Basel, Switzerland, and observed that since urban/built-up areas have higher albedo, their net radiation (Q^*) is lowest and therefore, the available energy for the heat fluxes is smaller. Due to this reason, during daytime, croplands have higher temperatures than settlements/industries.

However, the storage flux (Qs) of built material is much higher than that of vegetation in cropland which when accompanied with anthropogenic flux (QA) over-compensates negative net radiation during nighttime. Another factor is the Bowen ratio which indicates portioning between sensible and latent heat flux. Bowen ratio increases with a decrease in vegetation fraction. Hence, unless croplands are well grown and have moist soils due to irrigation, their Bowen ratio will remain high due to higher sensible heat flux which will lead to higher heat island intensities. Thus, croplands during the study period are likely to show higher values of heat island intensity than expected especially during the summer period.

- Role of soil moisture: Heat island development is determined by partitioning of surface energy balance between the built and non-built areas. An important feature to note about croplands in the study area is that the field

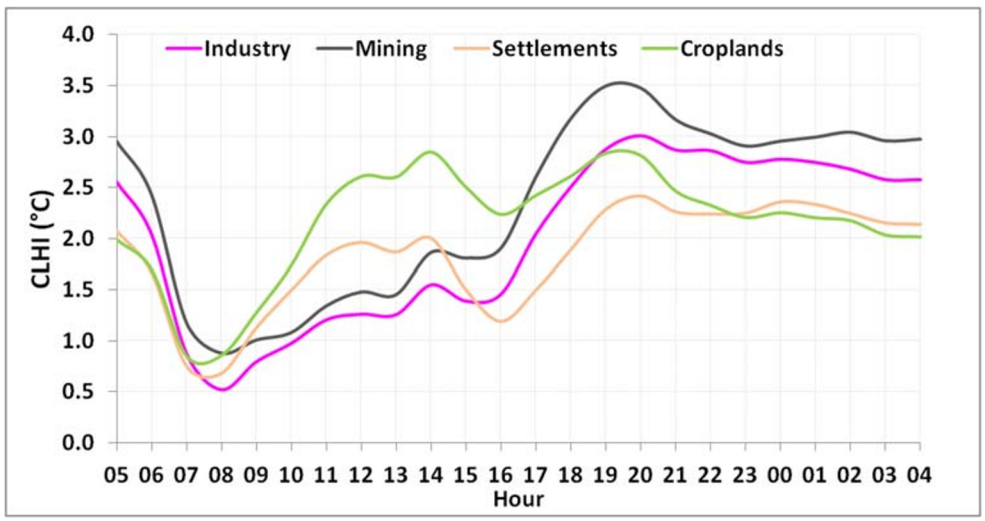

Fig. 4 Diurnal profile of in situ atmospheric heat island intensity (15 April–14 May 2016) [CLHI canopy-layer heat island intensity]

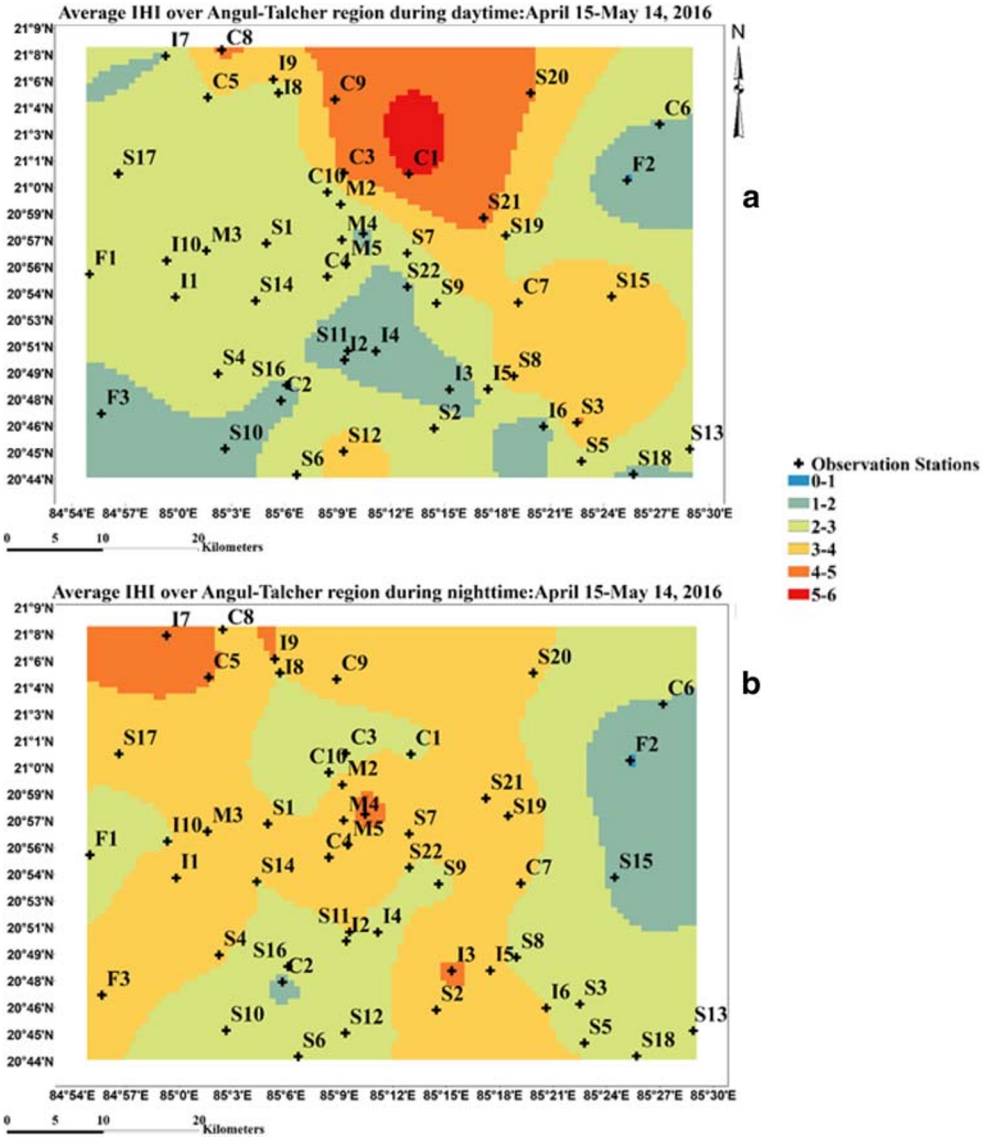

Fig. 5 Spatial variation of in situ atmospheric IHI intensity (°C) over Angul-Talcher region during **a** daytime and **b** nighttime for April 15–May 14, 2016 [I industry, M mining, S rural and urban settlements, C croplands, F forests]

observations were carried out during the non-active farming time. Thus, the soils of regions under croplands are dry, thereby having low thermal inertia. Lower thermal inertia of dry soils enables the greater rate of increase of soil surface temperature and hence higher warming of canopy air over croplands in daytime resulting in higher HINs in croplands in comparison with settlements or industrial areas. At night, the situation is reversed, when the positive values of the difference of urban-rural soil heat flux contribute to the positive UHI (Hafner and Kidder 1999) in the urban settlements.

During the daytime, industrial stations use a large amount of water for the industrial process as well as for daily purposes like gardening. Mining stations also used large water for coal washing and dust suppression. Industrial stations release anthropogenic heat during daytime which further increases the temperature in and around the administrative area. To overcome this issue, water is used as a coolant for reducing the temperature. Because of this, a small portion of water is evaporated in the atmosphere and the rest is again used for industrial purposes. This evaporated water vapor in the atmosphere will increase the latent heat flux in and around the industries during daytime (Rizwan et al. 2008). Similarly, in mining areas, water is used to suppress dust on gravel roads. Due to higher temperatures in mining stations, water evaporates during daytime and increases the moisture content in the area which further increases latent heat flux of mining stations. Thus, more moisture is present in the air in industry and mines than urban and rural settlement and cropland. Therefore, due to the above-mentioned reasons, a small drop in temperature was observed during daytime in industry and mining stations as compared with urban and rural settlements and croplands. It can be noted from Fig. 5a, b that stations such as Sirigida (C1)

and Godibandha (C3) observe maximum air temperature of more than 46 °C during daytime as compared with industrial and mining stations. Heat, which is trapped in built-up areas, is released during nighttime. Thus, the sensible heat flux is more in built-up areas as compared with cropland and forest. According to Terjung and Louie (1973), high structure systems such as industries absorb more than six times the solar radiation of nonurban plains during daytime which further radiates back the energy into the atmosphere during the cooling process at nighttime. It is also well documented that moist soil has more heat capacity than dry soil that absorbs more heat during daytime and releases during nighttime (Roxy et al. 2014; Alonge et al. 2007; Nobel and Geller 1987). Thus, water spread over roads and mining areas for coal washing and dust suppression results in high temperatures during nighttime and low temperature during daytime (Kissell 2003; Suez 2015).

- Urban-rural differences in thermal admittance: Another factor that is also related to soil heat flux as explained above is thermal admittance, which is a function of thermal conductivity and heat capacity. Materials that comprise the built-up mosaic generally have high thermal admittance; that is, they store or release energy at lower rates compared with soils in rural areas, resulting in a more conservative thermal climate; that is, built materials impact temperature of surrounding air at slower rate and hence rate of change of temperature is lower in built-up areas in comparison with open rural areas.

  i. The urban fabric cools off gradually in nighttime leading to urban heat island formation.
  ii. In daytime, urban areas also store energy at lower rates compared with cropland soils in rural areas (Chow and Roth 2006).
  iii. Consequently, during the daytime, industrial, mining, and urban and rural settlements stations that are entwined with steel, bricks and other construction material have less specific heat capacity. These materials absorb less heat and emit more heat but during the daytime. Water is used as an industrial agent in the industrial process as well as in household work which increases the water content in and around the stations. Thus, low IHI intensity is observed during daytime as compared with stations in croplands which has a much higher warming rate compared with the industrial stations. Consequently, this further results in a rapid increase of heat island intensity for the major part of the day over croplands in comparison with other LULCs.

- *Diurnal variation in the atmospheric boundary layer* (*ABL*): The ABL is defined as the turbulent layer of the atmosphere closest to the Earth's surface.

  i. At night, the rural ABL cools and can be relatively shallow (~ 100 m). On the other hand, the urban nocturnal ABL remains substantially deeper (~ 400 m) because it remains supplied with heat stored in buildings during the day (the storage or ground heat flux).
  ii. The difference between the thin rural ABL and the thick urban ABL causes a difference in heating rates between the urban and the rural environment in the early morning. Following daybreak, as rural areas have a higher warming rate (Chow and Roth 2006), the countryside will warm up faster than the urban environment since the layer overlying the countryside is thinner and has a lower volume than the urban ABL.
  iii. The larger heating rate in the rural environment causes the rural temperature to become higher than the urban temperature in the morning. This causes the initial nighttime UHI to shift to an urban cool island (UCI) effect approximately 4–5 h after sunrise (Theeuwes et al. 2015).

- *Effect of building infrastructure*:

  i. During nighttime, building canopy (sky view factor) acts as a means of trapping outgoing radiation.
  ii. However, during the daytime, it blocks incoming radiation which further leads to slower warming of industrial stations. Thus, bare ground (or uncultivated croplands as in the present case) becomes the main component of high-temperature areas (Zhang et al. 2007).

- The *presence of vegetation in industries* makes it cooler than urban areas (Chow and Roth 2006; Dousset et al. 2011). It is possible that the immediate areas around the built-up are experiencing advection of cooler air from the surrounding green spaces, lowering UHI intensity (Chow and Roth 2006).
- *Anthropogenic heat*: Round-the-clock activities led to higher HINs in mining stations during nighttime despite having no urban infrastructural fabric. Similarly, industrial sites also have round-the-clock operations.

4.3 Surface heat island intensities

Figure 6 displays box plots of surface heat island intensities for different LULCs for the 3 months of field campaign during nighttime. As in Fig. 2, the box represents the interquartile range; that is, the first quartile to the third quartile and the line within the box denotes the median. Ends of the line going through the box indicate minimum and maximum. The dots represent the mean value. During the first month, industry, mining, and settlement stations have similar mean HINs while

croplands have marginally higher mean HINs. However, for the second and third months, mining stations observed the highest surface HINs. There is no specific trend in the daytime too which can be seen in Fig. 7. While mining stations record higher HINs, the trend of other LULCs varies in all 3 months. Thus, there is a large variation in heat island intensities for each LULC. In other words, no LULC has any distinct features in terms of surface HIN statistics. A major reason for this could be attributed to the fact that in situ measurements of land surface temperatures may be influenced by certain limitations. There are certain issues that need to be considered before analyzing surface heat island intensities. Sensors measuring air temperature can be calibrated on-site against a standard instrument psychrometer and validated against available routine measurements. However, it is not simple to calibrate LST sensors on-site. In order to validate the surface measurements, the most often used method is that of comparison with satellite-derived data for land surface temperature. Thus, there are various sources of uncertainty in surface temperature measurements.

- There is a substantial difference between the variation of canopy air temperature with height and surface temperature gradient with respect to the depth below the surface. While this depends mainly on soil type, time of the year, and other features, a difference of depth of even a few millimeters in the placement of sensors can produce varying results. Hence, while canopy temperature sensors can be placed at a height varying from 1.5 to 2 m above the surface, ground temperature sensors have to be placed with precision at just below the surface and this uncertainty may also introduce some error.
- Satellite-derived data is in the form of a pixel average value which depends on the resolution of a sensor of the satellite. For instance, MODIS Terra/Aqua land surface temperature data product is available at a resolution of 1 km^2. Thus, a comparison of in situ point measurement with satellite-derived 1-km^2 area average land surface temperature is a point versus area average values of temperature and might lead to a close approximation but not necessarily correct comparative analysis. Further, a comparison with satellite data is possible with only two times during a day depending on passage time of the satellite against hourly data with 5-min averages for in situ measurements.
- LST measurements are more sensitive and prone to fluctuations than air temperature measurements in terms of surrounding spatial influence also due to higher thermal conductivity of the ground surface and any activity in the vicinity of an LST sensor will affect the measurement to a greater degree than that of an air temperature sensor.
- For in situ observations, field thermal emissivity depends on homogeneousness of the site whereas in satellite-derived measurements, emissivity depends upon multiple factors such as spatial roughness, physical property and wavelength, zenith angle, and other measuring conditions. The present study uses MODIS Aqua land surface temperature (LST) data product for comparison with in situ observations. Zhang et al. (2014) observed that MODIS data product has shown a strong agreement with the in situ observations which was observed at many stations in the present study too, barring a few where in situ LSTs were greater than 60 °C. Li et al. (2013) discussed the problems of estimating LST from

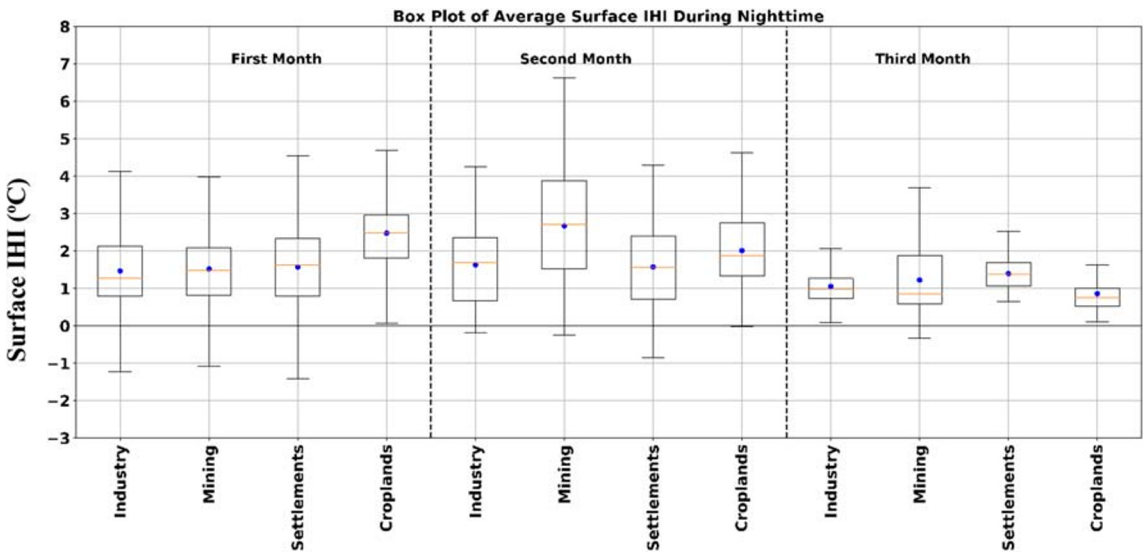

Fig. 6 Box plot of in situ surface heat island intensities during nighttime [first month: 15 April–14 May 2016, second month: 15 May–14 June 2016, third month: 15 June–14 Jul 2016]

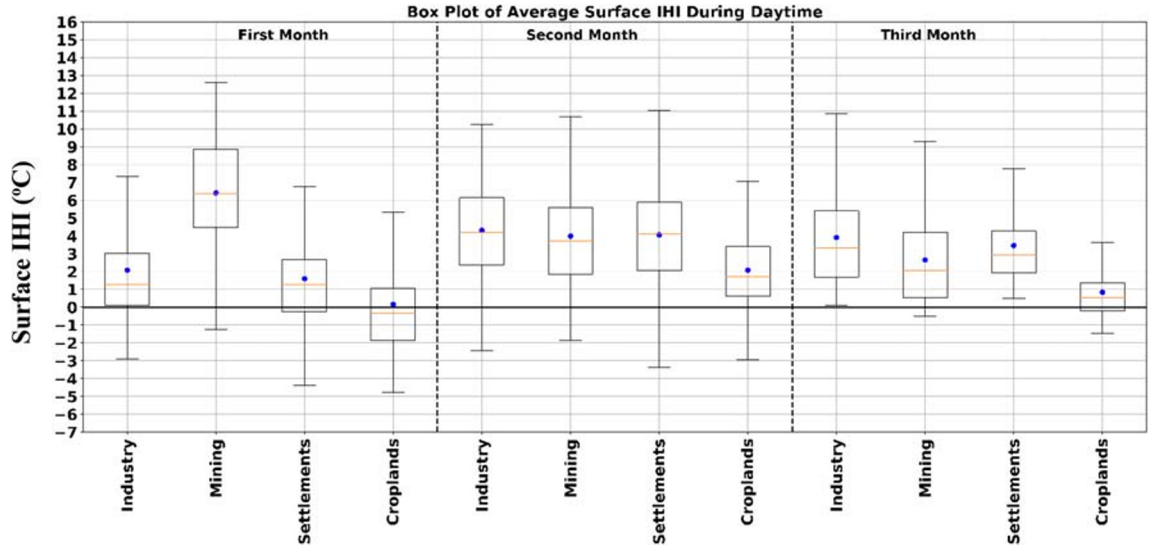

Fig. 7 Box plot of in situ surface heat island intensities during daytime [first month: 15 April–14 May 2016, second month: 15 May–14 June 2016, third month: 15 June–14 July 2016]

thermal infrared data of satellite sensors. The satellite-derived temperature has an unclear physical meaning, especially over heterogeneous and non-isothermal surfaces. The definition of the LST depends on that of the land surface emissivity because LST and land surface emissivity are coupled together in the total radiance. However, natural surfaces observed from space are usually heterogeneous. It is not unusual for the LST to vary by more than 10 K over just a few centimeters of distance or by more than 1 K in less than a minute over non-homogenous cover types. Appropriately scaling the satellite-derived LSTs to those measured at ground level, therefore, becomes difficult as it is not always feasible to find a homogeneous region as large as the satellite pixel size.

With these limitations, the most feasible way of validating measurements is to compare the difference between in situ measurements and satellite-derived data (MODIS Aqua) and eliminate stations with higher deviations within in situ MODIS LSTs. Figure 8 shows the average monthly difference between land surface temperatures of each station measured in situ and derived from the MODIS Aqua satellite.

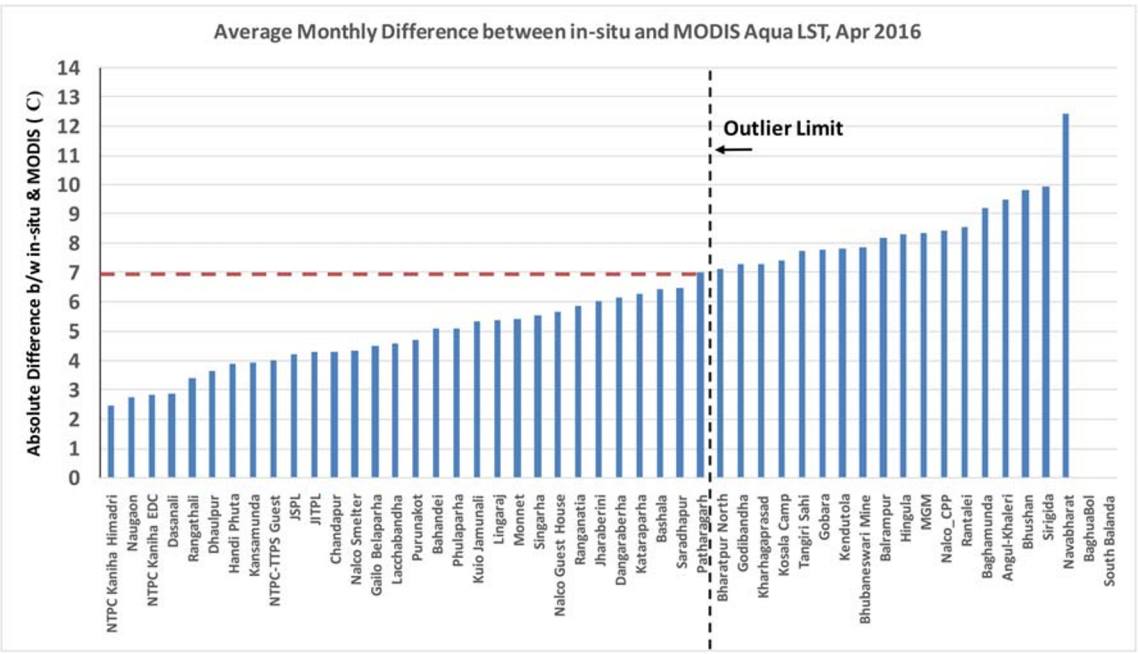

Fig. 8 Station-wise difference between in situ and satellite-derived LSTs

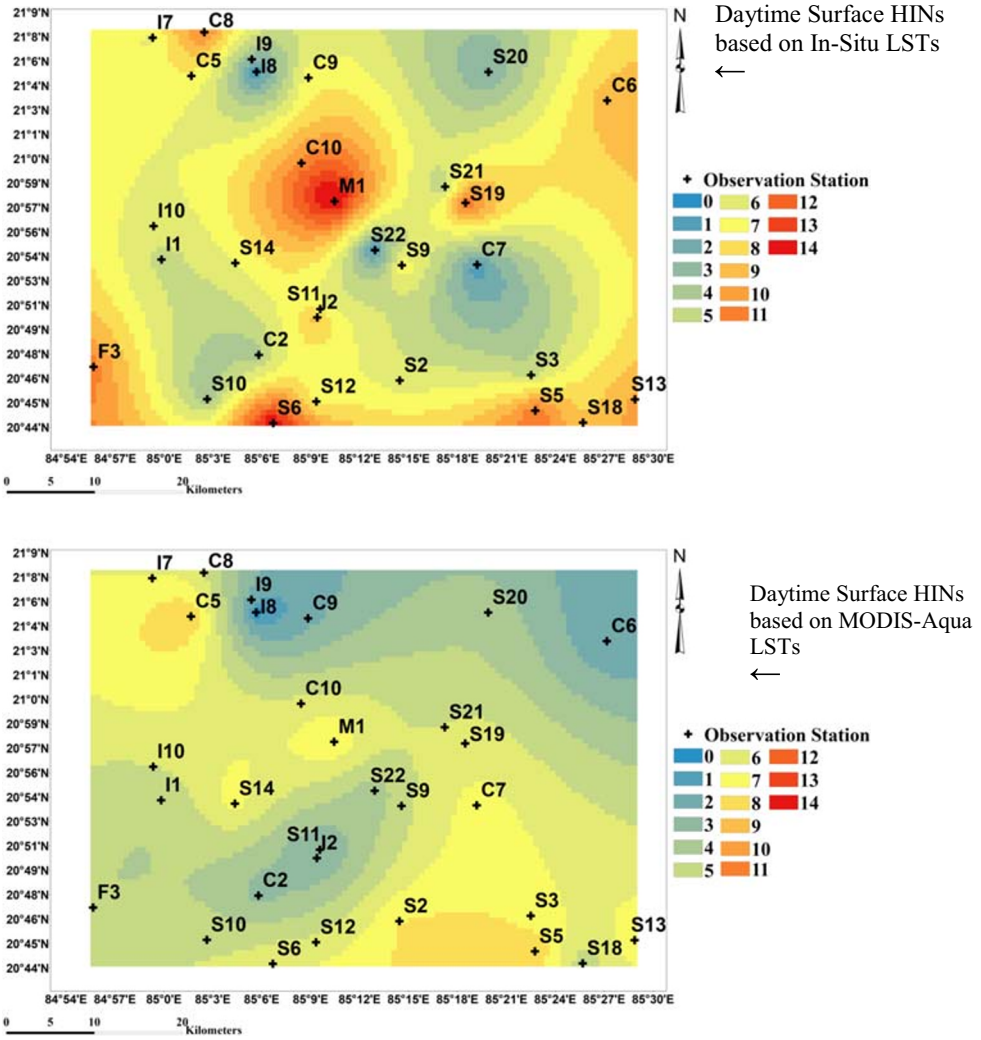

Fig. 9 Comparison of spatial distribution [top: in situ; bottom: MODIS Aqua] of daytime surface HINs (°C) (April 15–May 14) [I industry, M mining, S rural and urban settlements, C croplands, F forests]

Sites such as Sirigida, Baghamunda, Kendutola, TangiriSahi, Kharhagaprasad, and Godibandha in which sensors were either lost or damaged during the latter part of the experimental period show higher deviation in comparison with MODIS LSTs (> 7 °C). In general, industries and settlements were found to be most consistent and forest sites were found to have the highest differences in in situ and MODIS LSTs ranging from 6.5 to 9.2 °C.

Based on Fig. 8, the first 30 sites (up to deviation of 7 °C) were considered for comparison with satellite-derived observations. LULC averaged surface HINs were computed again for stations with least in situ satellite deviations in LSTs for nighttime and daytime corresponding to the passage of the MODIS Aqua satellite (0130 h and 1330 h local time). In this case, forest sites were not taken as reference points. The minimum temperature amongst non-industrial/non-mining stations was taken as the reference temperature. Further, in view of limitations as discussed above, we have focused on HIN trends amongst various LULC between satellite data and in situ data rather than magnitudes of heat island intensities. Table 3 consists of different observation stations to analyze the difference between in situ and satellite-derived LSTs.

Figure 9 shows a comparison of daytime spatial surface HINs from in situ and satellite-derived LSTs averaged over the duration of the first month of field campaign (15 April 14 May). The zone which includes the industrial site of JITPL and croplands of Kansamunda and Jharaberini is a common hotspot in both distributions. Further, settlements such as Handiphuta and Bawanda are also common hotspots of surface HINs. A common cool island is also observed which includes NTPC Kaniha and EDC. Figure 10 shows a comparison of spatial surface HINs from in situ and satellite-derived LSTs for nighttime. The zone including JITPL-Kansamunda-Jharaberini continues to remain a common hotspot during nighttime as well. Sites of Handiphuta and Bawandha (settlements) and Ranganathia and Sirigida (croplands) are also in higher ranges of HINs and spatial distributions of both in situ and MODIS satellite HINs. Overall, in situ and satellite HINs are closer in magnitude during nighttime in comparison with daytime which has been observed in earlier studies also

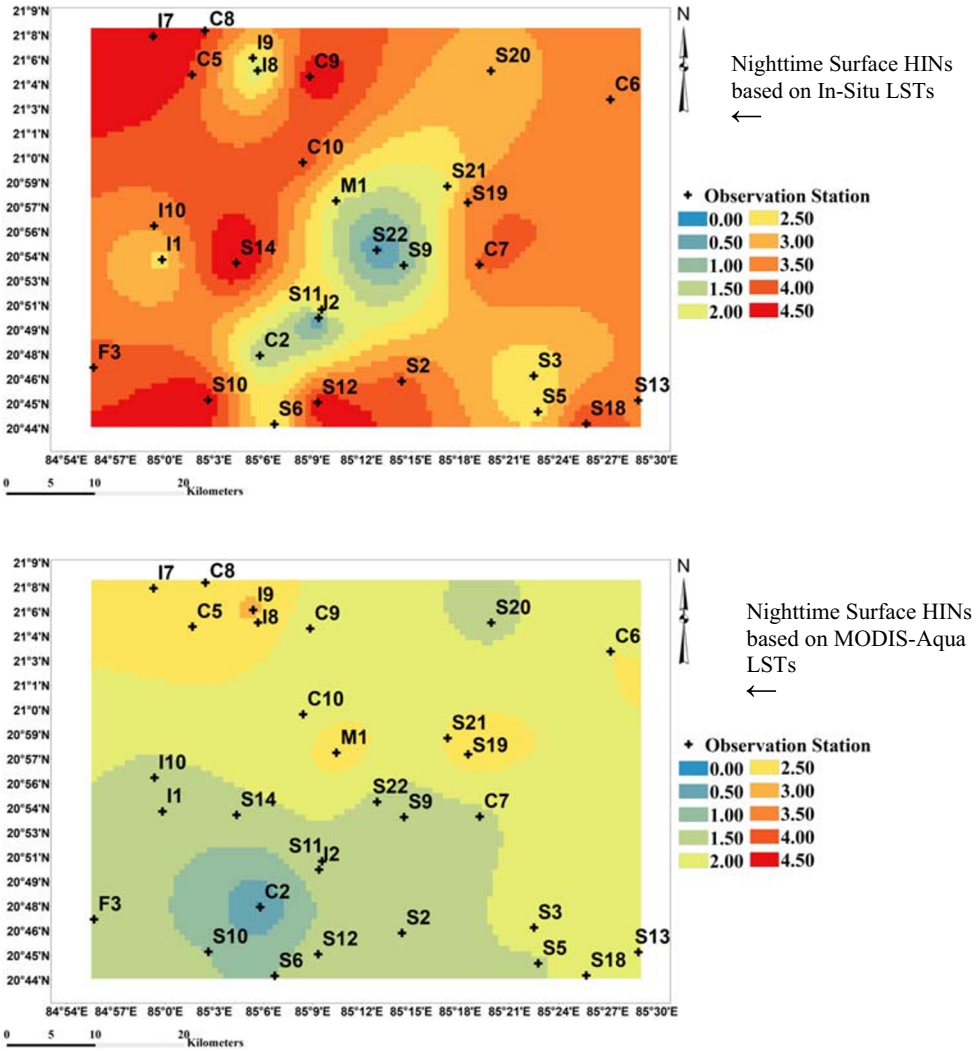

Fig. 10 Comparison of spatial distribution [top: in situ; bottom: MODIS Aqua] of nighttime surface HINs (°C) (April 15–May 14) [I industry, M mining, S rural and urban settlements, C croplands, F forests]

(Mohan et al. 2012). The difference arises mainly due to point to area average comparison which gets accentuated during the daytime.

Table 5 shows monthly mean values of average surface HIN for the first month (April 15–May 14) of field campaign for each LULC after eliminating outlier stations. The results are shown here for the first month only because in situ measurements of the early days were least affected by limitations and errors.

The present study assesses both canopy and surface heat islands. However, these two phenomena cannot be equated to draw out common inferences. There is no simple general relationship available between the surface and air temperatures. Without considering the differing source areas for the two measurements and atmospheric effects that affect air temperatures (such as radiative divergence in the urban canopy layer and horizontal heat advection), it is easy to misinterpret canopy-layer UHIs vis-a-vis measurements of surface temperatures (Roth 2013). In view of this, most UHI studies examine air temperatures in urban areas (IAUC 2017). Considering that canopy-layer heat island–related field experiments are not feasible to conduct most of the time, researchers, at times, resort to utilizing satellite-derived LST to draw inference for UHI in a given area. However, the most studied urban heat island is that in the canopy-layer air which is most easily accessed for measurements and represents air volume in which bulk of human/urban activities occur (Voogt 2017). Hence, in terms of mitigation aspects too, researchers design and analyze mitigation measures for canopy-layer UHIs. Nonetheless, a comprehensive analysis of heat island intensities has been presented in the present study combining in situ air and surface temperatures as well as satellite-derived observations.

5 Conclusions

A field campaign was carried out to study the heat island phenomenon in the industrial zone of Angul-Talcher in the tropical region of south-east India. Measurements were

Table 5 Comparison of monthly average surface HINs (°C) for each LULC

LULC	Daytime		Nighttime	
	In situ (rank out of 5)	Satellite (rank out of 5)	In situ (rank out of 5)	Satellite (rank out of 5)
Industry	5.2 (4)	2.3 (4)	2.7 (3)	1.4 (2)
Mining	6.3 (3)	2.9 (3)	2.2 (4)	1.9 (1)
Settlements	8.1 (1)	4.4 (1)	3.4 (2)	1.0 (4)
Croplands	7.4 (2)	3.4 (2)	4.0 (1)	1.2 (3)
Ranking	1. Settlements 2. Croplands 3. Mining 4. Industry	1. Settlements 2. Croplands 3. Mining 4. Industry	1. Croplands 2. Settlements 3. Industry 4. Mining	1. Mining 2. Industry 3. Croplands 4. Settlements
Remarks on ranking	LULCs in both in situ and satellite data have similar trends		Different trends observed in in situ and satellite data	
Common hotspots (both satellite and in situ)	Kansamunda (cropland), Puranakot (settlement) Handiphuta (settlement)		Industry: JITPL, NTPC KanihaHimgiri, NTPC Kaniha; EDC cropland: Kansamunda, Singarha	

conducted for a period of 3 months (April 15, 2016, to July 14, 2016) at several observation stations under different LULCs.

The major conclusions of the study area as follows:

- Mean nighttime atmospheric heat island intensities (averaged over the 3-month duration of field measurements) amongst different LULCs were observed to be in the following order: mining sites (2.74 °C) > industry (2.52 °C) > rural and urban settlements (2.13 °C) and croplands (2.06 °C). Round-the-clock activities led to higher HINs in mining stations during nighttime despite having no urban fabric.

- During the daytime, croplands experienced highest mean atmospheric HIN (2.07 °C) followed by mining sites (1.7 °C), settlements (1.68 °C), and industrial stations (1.45 °C). Croplands observing the most frequent atmospheric HIN hotspots during daytime can be attributed to low moisture of the soils during the non-farming period of the field campaign.

- Settlements and croplands have higher daytime surface HINs in both in situ and satellite-derived measurements. Mean daytime surface IHIs amongst different LULCs were observed to be in the following order: mining sites (4.89 °C) > industry (3.77 °C) > settlements (3.70 °C) > cropland (1.09), while mean nighttime surface IHIs amongst different LULCs were observed to be in the following order: mining sites (2.77 °C) > industry (2.65 °C) > urban and rural settlements (2.17 °C) > cropland (2.09).

- Comparison of in situ surface IHIs with satellite-derived LST-based IHIs revealed that in situ and satellite-derived surface HINs are closer in magnitude during nighttime in comparison with daytime.

In the present study, the monthly maximum heat island intensities (HINs), 3-month mean HINs, and hourly maximum HINs both during daytime and nighttime are examined in Angul-Talcher region which are assessed to be comparable with urban city centers in Asian cities with the prolific built environment and associated heat emissions therein. Hence, this study provides evidence about how similar intensity heat island effects can be observed in an industrial zone too despite having the comparatively lesser density of built-up structures. In the context of highly industrialized regions, this study is one of the first few of its kind to include an extensive field campaign for a core industrial area to examine the heat island effect and also provide a comparative assessment with satellite-derived observations.

Acknowledgments

We sincerely acknowledge the initiative undertaken by the officials of Odisha State Pollution Control Board, State of Odisha, India (Shri Asit Kumar Tripathy (Chairman), Shri R. Balakrishnan (Former Chairman), Shri Debidutta Biswal (Member Secretary), Shri Rajeev Kumar (Former Member Secretary)) for getting this study conceptualized and operationalized through the project "Heat Island Study in Angul-Talcher Area of Odisha" (HISAT) in collaboration with Indian Institute of Technology Delhi via sanction order no. 17785 dated 07 November 2015 under the Climate Change Action Plan of State of Odisha. We gratefully acknowledge the advice and time-to-time guidance in the study and facilitating data and industry support from various officials of State Pollution Control Board, Odisha, such as Ms. Subhadasini Das (Deputy Environmental Engineer), Mr. Bijaya Kumar Bhoi (Asst. Environmental Engg), and Dr. B. B. Dash (R.O, SPCB, Angul, Odisha). The assistance of students, research scholars, and project staff of Centre for Atmospheric Sciences, IIT Delhi, namely Dr. Medhavi Gupta, Dr. Sourangsu Chowdhary, Dr. Preeti Gunwani, and Mr. Rahul Jain is also

appreciated. We are thankful to the staff of Visiontek Consultancy Services Private Limited (VCSPL), Bhubaneswar, Odisha (Mr. P. Kumar Ranjan (Managing Director), Mr. Niranjan Lal Aggarwal (Director), Mr. Ashish Sahu, Mr. Prabhakar Mishra, Mr. Bijay Sahu, and Mr. Tapas) for incessantly supporting the field campaign and related logistical issues. We are especially thankful to all officials affiliated with industries, coal mines, government, and non-government sectors of India and city and village dwellers that have supported and helped with field campaign, data collection, and installation and security of weather stations at their respective residences.

References

Alonge CJ, Mohr KI, Tao W-K (2007) Numerical studies of wet versus dry soil regimes in the west African Sahel. J Hydrometeorol 8:102–116. https://doi.org/10.1175/jhm559.1

Amirtham LR (2016) Urbanization and its impact on urban heat island intensity in Chennai Metropolitan Area. India Indian J Sci Technol 9. https://doi.org/10.17485/ijst/2016/v9i5/87201

Azevedo J, Chapman L, Muller C (2016) Quantifying the daytime and night-time urban heat island in Birmingham, UK: a comparison of satellite derived land surface temperature and high resolution air temperature observations. Remote Sens 8:153. https://doi.org/10.3390/rs8020153

Babazadeh M, Kumar P (2015) Estimation of the urban heat island in local climate change and vulnerability assessment for air quality in Delhi. Eur Sci J 1:55–65. https://eujournal.org/index.php/esj/article/view/5712/5518

Barlow JF, Halios CH, Lane SE, Wood CR (2015) Observations of urban boundary layer structure during a strong urban heat island event. Environ Fluid Mech 15:373–398. https://doi.org/10.1007/s10652-014-9335-6

Bokaie M, Zarkesh MK, Arasteh PD, Hosseini A (2016) Assessment of urban heat island based on the relationship between land surface temperature and land use/ land cover in Tehran. Sustain Cities Soc 23:94–104. https://doi.org/10.1016/j.scs.2016.03.009

Bokwa A, Hajto MJ, Walawender JP, Szymanowski M (2015) Influence of diversified relief on the urban heat island in the city of Kraków, Poland. Theor Appl Climatol 122:365–382. https://doi.org/10.1007/s00704-015-1577-9

Central Pollution Control Board (CPCB) (2010) Annual Report 2009–10. http://www.cpcbenvis.nic.in/annual_report/AnnualReport_40_Annual_Report_09-10.pdf. Accessed 15 Apr 2019

Chow WTL, Roth M (2006) Temporal dynamics of the urban heat island of Singapore. Int J Climatol 26:2243–2260. https://doi.org/10.1002/joc.1364

Christian EI (2013) Mapping Enugu city's urban heat island. Int J Environ Prot Policy 1:50. https://doi.org/10.11648/j.ijepp.20130104.12

Dousset B et al (2011) Satellite monitoring of summer heat waves in the Paris metropolitan area. Int J Climatol 31:313–323. https://doi.org/10.1002/joc.2222

Gallo KP (2002) Satellite-based detection of global urban heat-island temperature influence. J Geophys Res 107. https://doi.org/10.1029/2002JD002588

Grover A, Singh R (2015) Analysis of urban heat island (UHI) in relation to normalized difference vegetation index (NDVI): a comparative study of Delhi and Mumbai. Environments 2:125–138. https://doi.org/10.3390/environments2020125

Hafner J, Kidder SQ (1999) Urban heat island modeling in conjunction with satellite-derived surface/soil parameters. J Appl Meteorol 38:448–465. https://doi.org/10.1175/1520-0450(1999)038<0448:UHIMIC>2.0.CO;2

Hu L, Brunsell NA (2015) A new perspective to assess the urban heat island through remotely sensed atmospheric profiles. Remote Sens Environ 158:393–406. https://doi.org/10.1016/j.rse.2014.10.022

International Association for Urban Climate (IAUC) (2017) The urban canopy layer heat island. http://www.urban-climate.org/UHI_Canopy.pdf. Accessed 15 Apr 2019

Jha N (2015) Coal mining and rural ecology: a study in Talcher. Odisha. 61

Joshi R, Raval H, Pathak M et al (2015) Urban heat island characterization and isotherm mapping using geo-informatics technology in Ahmedabad City, Gujarat State, India. Int J Geosci 06:274–285. https://doi.org/10.4236/ijg.2015.63021

Kaplan G, Avdan U, Avdan ZY (2018) Urban heat island analysis using the Landsat 8 satellite data: a case study in Skopje, Macedonia. Proceedings 2:358. https://doi.org/10.3390/ecrs-2-05171

Khan A, Chatterjee S (2016) Numerical simulation of urban heat island intensity under urban–suburban surface and reference site in Kolkata. India Model Earth Syst Environ 2:1–11. https://doi.org/10.1007/s40808-016-0119-5

Kikon N, Singh P, Singh SK, Vyas A (2016) Assessment of urban heat islands (UHI) of Noida City, India using multi-temporal satellite data. Sustain Cities Soc 22:19–28. https://doi.org/10.1016/j.scs.2016.01.005

Kissell FN (2003) Handbook for dust control in mining

Leconte F, Bouyer J, Claverie R, Pétrissans M (2015) Using local climate zone scheme for UHI assessment: evaluation of the method using mobile measurements. Build Environ 83:39–49. https://doi.org/10.1016/j.buildenv.2014.05.005

Li X, Hong C, Yuan L, Cai Y (2012) Observing the urban heat island in summer from city center to fringe 2014: taking Wuhan as an example. In: 2012 International Conference on Green and Ubiquitous Technology. IEEE, Bandung, pp 33–36

Li Z-L et al (2013) Satellite-derived land surface temperature: current status and perspectives. Remote Sens Environ 131:14–37. https://doi.org/10.1016/j.rse.2012.12.008

Li X, Gong P, Liang L (2015) A 30-year (1984–2013) record of annual urban dynamics of Beijing City derived from Landsat data. Remote Sens Environ 166:78–90. https://doi.org/10.1016/j.rse.2015.06.007

Mallick J, Rahman A, Singh CK (2013) Modeling urban heat islands in heterogeneous land surface and its correlation with impervious surface area by using night-time ASTER satellite data in highly urbanizing city, Delhi-India. Adv Space Res 52:639–655. https://doi.org/10.1016/j.asr.2013.04.025

Maral SG, Mukhopadhyay T (2015) Signal of urban heat island (UHI) effect : a case study of Mumbai metropolitan region. 12

Mathew A, Chaudhary R, Gupta N et al (2015) Study of urban heat island effect on Ahmedabad City and its relationship with urbanization and vegetation parameters. Math Sci 4:10

Mishra N, Das N (2017) Coal mining and local environment: a study in Talcher coalfield of India. Air Soil Water Res 10:117862211772891. https://doi.org/10.1177/1178622117728913

Mohan M, Kikegawa Y, Gurjar BR, et al (2009) Assessment of urban heat island intensities over Delhi 4

Mohan M, Kikegawa Y, Gurjar BR et al (2012) Urban heat island assessment for a tropical urban airshed in India. Atmospheric Clim Sci 02:127–138. https://doi.org/10.4236/acs.2012.22014

Mohan M, Kikegawa Y, Gurjar BR et al (2013) Assessment of urban heat island effect for different land use–land cover from micrometeorological measurements and remote sensing data for megacity Delhi.

Theor Appl Climatol 112:647–658. https://doi.org/10.1007/s00704-012-0758-z

Montavez JP, Rodriguez A, Jimenez JI (2000) A study of the urban heat island of Granada. Int J Climatol 20:899–911. https://doi.org/10.1002/1097-0088(20000630)20:8<899::AID-JOC433>3.0.CO;2-I

Morini E, Castellani B, Presciutti A et al (2017) Experimental analysis of the effect of geometry and facade materials on urban district's equivalent albedo. Sustainability 9:1245. https://doi.org/10.3390/su9071245

Nobel PS, Geller GN (1987) Temperature modelling of wet and dry desert soils. J Ecol 75:247–258. https://doi.org/10.2307/2260549

Oke TR (1973) City size and the urban heat island. Atmospheric Environ 7:769–779. https://doi.org/10.1016/0004-6981(73)90140-6

Pandey P, Kumar D, Prakash A, Masih J, Singh M, Kumar S, Jain VK, Kumar K (2012) A study of urban heat island and its association with particulate matter during winter months over Delhi. Sci Total Environ 414:494–507. https://doi.org/10.1016/j.scitotenv.2011.10.043

Parishwad OG, Shinkar V (2017) Critical review of the climate change impact on urban areas by assessment of heat island effect. Case of Pune, India 8

Parlow E, Scherer D, Beha H-D, Goßmann H, Braun H-M (1996) Urban climatological parameters derived from ERS-1 & LANDSAT-TM multisensor data. In: ERS Applications, 1996. p 173. http://articles.adsabs.harvard.edu/pdf/1996ESASP.383..173P. Accessed 16 Apr 2019

Peron F, De Maria MM, Spinazzè F, Mazzali U (2015) An analysis of the urban heat island of Venice mainland. Sustain Cities Soc 19:300–309. https://doi.org/10.1016/j.scs.2015.05.008

Ramamurthy P, González J, Ortiz L et al (2017) Impact of heatwave on a megacity: an observational analysis of New York City during July 2016. Environ Res Lett 12:054011. https://doi.org/10.1088/1748-9326/aa6e59

Rizwan AM, Dennis LYC, Liu C (2008) A review on the generation, determination and mitigation of Urban Heat Island. J Environ Sci 20:120–128. https://doi.org/10.1016/S1001-0742(08)60019-4

Roth M (2013) Urban heat islands. In: Fernando HJS (ed) Handbook of environmental fluid dynamics, vol. 2. CRC Press/Taylor & Francis Group, LLC, Boca Raton, pp 143–159

Roxy MS, Sumithranand VB, Renuka G (2014) Estimation of soil moisture and its effect on soil thermal characteristics at astronomical observatory, Thiruvananthapuram, South Kerala. J Earth Syst Sci 123:1793–1807. https://doi.org/10.1007/s12040-014-0509-x

Saaroni H, Ziv B (2010) Estimating the urban heat island contribution to urban and rural air temperature differences over complex terrain: application to an arid city. J Appl Meteorol Climatol 49:2159–2166. https://doi.org/10.1175/2010JAMC2473.1

Sahu S, Pawar A, Mukherjee M (2014) Urban heat island investigation: techniques and methods so far 7

Santamouris M (2015) Analyzing the heat island magnitude and characteristics in one hundred Asian and Australian cities and regions. Sci Total Environ 512–513:582–598. https://doi.org/10.1016/j.scitotenv.2015.01.060

Sarkar A, De Ridder K (2011) The urban heat island intensity of Paris: a case study based on a simple urban surface parametrization. Bound-Layer Meteorol 138:511–520. https://doi.org/10.1007/s10546-010-9568-y

Sastry M, Kumar Varma H, Halve V (2017) Urban planning characteristics to mitigate climate change in context of urban heat island effect. http://www.teriin.org/sites/default/files/2018-03/urba-heat-island-effect-report.pdf

Sismanidis P, Keramitsoglou I, Kiranoudis CT (2015) A satellite-based system for continuous monitoring of surface urban heat islands. Urban Clim 14:141–153. https://doi.org/10.1016/j.uclim.2015.06.001

Soltani A, Sharifi E (2017) Daily variation of urban heat island effect and its correlations to urban greenery: a case study of Adelaide. Front Archit Res 6:529–538. https://doi.org/10.1016/j.foar.2017.08.001

Song X-P, Sexton JO, Huang C et al (2016) Characterizing the magnitude, timing and duration of urban growth from time series of Landsat-based estimates of impervious cover. Remote Sens Environ 175:1–13. https://doi.org/10.1016/j.rse.2015.12.027

Srivastava AK, Voogt J, Kshirsagar SR, Srivastava K (2016) Heat islands over Mumbai as revealed by autorecorded thermograph data. J Earth Syst Sci 125:85–93. https://doi.org/10.1007/s12040-015-0648-8

Suez (2015) Water technologies & solutions: more dust control, less water. https://www.suezwatertechnologies.com/kcpguest/documents/...Cust/.../TP1205EN.pdf

Swain D, Roberts GJ, Dash J, Lekshmi K, Vinoj V, Tripathy S (2017) Impact of rapid urbanization on the City of Bhubaneswar, India. Proc Natl Acad Sci India Sect Phys Sci 87:845–853. https://doi.org/10.1007/s40010-017-0453-7

Taha H (2017) Characterization of urban heat and exacerbation: development of a heat island index for California. Climate 5:59. https://doi.org/10.3390/cli5030059

Tan J, Yang L, Grimmond CSB et al (2015) Urban integrated meteorological observations: practice and experience in Shanghai, China. Bull Am Meteorol Soc 96:85–102. https://doi.org/10.1175/BAMS-D-13-00216.1

Terjung WH, Louie SS-F (1973) Solar radiation and urban heat islands. Ann Assoc Am Geogr 63:181–207. https://doi.org/10.1111/j.1467-8306.1973.tb00918.x

Theeuwes NE, Steeneveld G-J, Ronda RJ et al (2015) Cool city mornings by urban heat. Environ Res Lett 10:114022. https://doi.org/10.1088/1748-9326/10/11/114022

Tomlinson CJ, Chapman L, Thornes JE, Baker CJ (2012) Derivation of Birmingham's summer surface urban heat island from MODIS satellite images. Int J Climatol 32:214–224. https://doi.org/10.1002/joc.2261

Toparlar Y, Blocken B, Vos P et al (2015) CFD simulation and validation of urban microclimate: a case study for Bergpolder Zuid, Rotterdam. Build Environ 83:79–90. https://doi.org/10.1016/j.buildenv.2014.08.004

Tran H, Uchihama D, Ochi S, Yasuoka Y (2006) Assessment with satellite data of the urban heat island effects in Asian mega cities. Int J Appl Earth Obs Geoinformation 8:34–48. https://doi.org/10.1016/j.jag.2005.05.003

van Hove LWA, Jacobs CMJ, Heusinkveld BG et al (2015) Temporal and spatial variability of urban heat island and thermal comfort within the Rotterdam agglomeration. Build Environ 83:91–103. https://doi.org/10.1016/j.buildenv.2014.08.029

Van Nguyen O, Kawamura K, Trong DP et al (2015) Temporal change and its spatial variety on land surface temperature and land use changes in the Red River Delta, Vietnam, using MODIS time-series imagery. Environ Monit Assess 187. https://doi.org/10.1007/s10661-015-4691-3

Voogt JA (2017) Urban Climatology. In: Richardson D, Castree N, Goodchild MF, Kobayashi A, Liu W, Marston RA (eds) International encyclopedia of geography, 15 volume set: people, the earth. Environment and Technology. Wiley, New York, p 7311

Wang Y, Akbari H (2015) Development and application of 'thermal radiative power' for urban environmental evaluation. Sustain Cities Soc 14:316–322. https://doi.org/10.1016/j.scs.2014.07.003

Wang Y, Berardi U, Akbari H (2015) The urban heat island effect in the city of Toronto. Procedia Eng 118:137–144. https://doi.org/10.1016/j.proeng.2015.08.412

Wang Y, Berardi U, Akbari H (2016) Comparing the effects of urban heat island mitigation strategies for Toronto, Canada. Energy Build 114:2–19. https://doi.org/10.1016/j.enbuild.2015.06.046

Wang K, Jiang S, Wang J et al (2017) Comparing the diurnal and seasonal variabilities of atmospheric and surface urban heat islands based on

the Beijing urban meteorological network: ATMOSPHERIC AND SURFACE UHI. J Geophys Res Atmospheres 122:2131–2154. https://doi.org/10.1002/2016JD025304

Weber S, Sadoff N, Zell E, de Sherbinin A (2015) Policy-relevant indicators for mapping the vulnerability of urban populations to extreme heat events: a case study of Philadelphia. Appl Geogr 63:231–243. https://doi.org/10.1016/j.apgeog.2015.07.006

Xie Q, Zhou Z (2015) Impact of urbanization on urban heat island effect based on tm imagery in Wuhan, China. Environ Eng Manag J 9

Yadav N, Sharma C, Peshin SK, Masiwal R (2017) Study of intra-city urban heat island intensity and its influence on atmospheric chemistry and energy consumption in Delhi. Sustain Cities Soc 32:202–211. https://doi.org/10.1016/j.scs.2017.04.003

Zhang L, Weng Q (2016) Annual dynamics of impervious surface in the Pearl River Delta, China, from 1988 to 2013, using time series Landsat imagery. ISPRS J Photogramm Remote Sens 113:86–96. https://doi.org/10.1016/j.isprsjprs.2016.01.003

Zhang J, Wang Y, Wang Z (2007) Change analysis of land surface temperature based on robust statistics in the estuarine area of Pearl River (China) from 1990 to 2000 by Landsat TM/ETM+ data. Int J Remote Sens 28:2383–2390. https://doi.org/10.1080/01431160701236811

Zhang Y, Li Z, Li J (2014) Comparisons of emissivity observations from satellites and the ground at the CRCS Dunhuang Gobi site: Comparisons of emissivity observations. J Geophys Res Atmospheres 119:13,026–13,041. https://doi.org/10.1002/2014JD022216

Zhibin R, Haifeng Z, Xingyuan H, Dan Z, Xingyang Y (2015) Estimation of the relationship between urban vegetation configuration and land surface temperature with remote sensing. J Indian Soc Remote Sens 43:89–100. https://doi.org/10.1007/s12524-014-0373-9

Zhou X, Chen H (2018) Impact of urbanization-related land use land cover changes and urban morphology changes on the urban heat island phenomenon. Sci Total Environ 635:1467–1476. https://doi.org/10.1016/j.scitotenv.2018.04.091

Zhu K, Bayer P, Grathwohl P, Blum P (2015) Groundwater temperature evolution in the subsurface urban heat island of Cologne, Germany: groundwater temperature evolution in the subsurface urban heat island. Hydrol Process 29:965–978. https://doi.org/10.1002/hyp.10209